frontiers | Frontiers in Cell and Developmental Biology

TYPE Original Research
PUBLISHED 31 March 2023
DOI 10.3389/fcell.2023.1104620

OPEN ACCESS

EDITED BY
Angelika Stollewerk,
Queen Mary University of London,
United Kingdom

REVIEWED BY
Bo Joakim Eriksson,
University of Vienna, Austria
Frank Smith,
University of North Florida, United States

*CORRESPONDENCE
Tiffany A. Cook,
tiffany.cook2@wayne.edu
Elke K. Buschbeck,
elke.buschbeck@uc.edu

†PRESENT ADDRESS
Mark Charlton-Perkins, Department of Biology, Miami University, Oxford, OH, United States

SPECIALTY SECTION
This article was submitted to Evolutionary Developmental Biology, a section of the journal Frontiers in Cell and Developmental Biology

RECEIVED 21 November 2022
ACCEPTED 13 March 2023
PUBLISHED 31 March 2023

CITATION
Rathore S, Meece M, Charlton-Perkins M, Cook TA and Buschbeck EK (2023), Probing the conserved roles of cut in the development and function of optically different insect compound eyes. *Front. Cell Dev. Biol.* 11:1104620. doi: 10.3389/fcell.2023.1104620

Probing the conserved roles of cut in the development and function of optically different insect compound eyes

Shubham Rathore[1], Michael Meece[1], Mark Charlton-Perkins[2†], Tiffany A. Cook[3]* and Elke K. Buschbeck[1]*

[1]Department of Biological Sciences, University of Cincinnati, Cincinnati, OH, United States, [2]Division of Developmental Biology and Department of Pediatric Ophthalmology, Cincinnati Children's Hospital Medical Center, Cincinnati, OH, United States, [3]Center of Molecular Medicine and Genetics, Department of Ophthalmological, Visual and Anatomical Sciences, Wayne State University School of Medicine, Detroit, MI, United States

Astonishing functional diversity exists among arthropod eyes, yet eye development relies on deeply conserved genes. This phenomenon is best understood for early events, whereas fewer investigations have focused on the influence of later transcriptional regulators on diverse eye organizations and the contribution of critical support cells, such as Semper cells (SCs). As SCs in *Drosophila melanogaster* secrete the lens and function as glia, they are critical components of ommatidia. Here, we perform RNAi-based knockdowns of the transcription factor *cut* (CUX in vertebrates), a marker of SCs, the function of which has remained untested in these cell types. To probe for the conserved roles of *cut*, we investigate two optically different compound eyes: the apposition optics of *D. melanogaster* and the superposition optics of the diving beetle *Thermonectus marmoratus*. In both cases, we find that multiple aspects of ocular formation are disrupted, including lens facet organization and optics as well as photoreceptor morphogenesis. Together, our findings support the possibility of a generalized role for SCs in arthropod ommatidial form and function and introduces Cut as a central player in mediating this role.

KEYWORDS

visual system development, invertebrates, optics, conserved gene networks, compound eyes, cone cells, semper cells

Introduction

Compound eyes, a prominent eye type in arthropods, are known for their typically highly organized multifaceted convex corneal lenses and underlying photoreceptor (PR) clusters that are components of precisely organized visual units (ommatidia). Despite sharing similar features, compound eye types show remarkable diversity, often related to the animal's ecology (Land and Nilsson, 2012; Cronin et al., 2014; Meece et al., 2021; Nilsson, 2021). Optically, compound eyes can be divided into two general types: Apposition and superposition (Nilsson, 1983; Nilsson, 1989; Meyer-Rochow, 2015). In the more ancestral apposition eye, each lens only serves its own underlying PRs, as exemplified in *D. melanogaster* (Figure 1A). Note that *Drosophila melanogaster* eyes are actually neural-superposition eyes, which refers to a neural (rather than optical) organization that allows pooling from neighboring units (Nilsson, 1989; Agi et al., 2014; Nilsson, 2021).

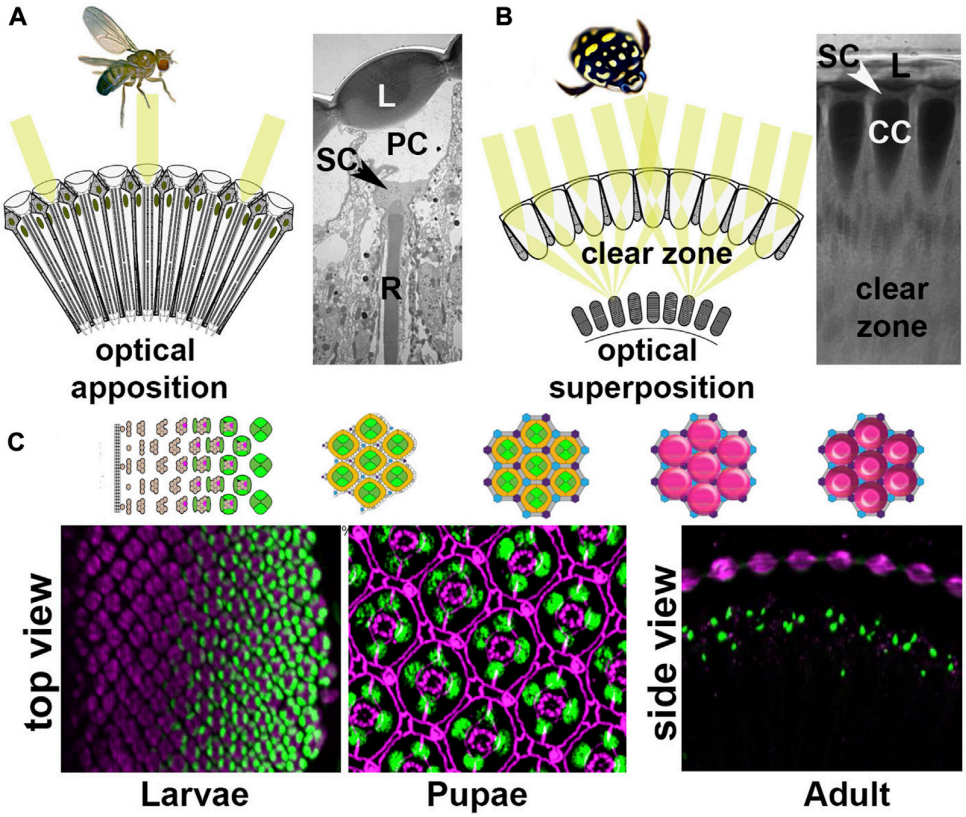

FIGURE 1
Compound eye types and development. **(A)** *D. melanogaster* has a neural-superposition eye, the optics of which follows typical apposition organization, with individual lenses (L) that each project a tiny image fragment onto the tips of underlying photoreceptor rhabdomeres (R). Underneath the lens, there is a pseudocone (PC) and four Semper cell (SC) bodies. **(B)** *T. marmoratus* has an optical superposition eye, in which sets of lenses synergistically project image points onto corresponding underlying closed rhabdoms. In this organization, the SC bodies are located in close proximity to the lens and above the photoreceptor cell bodies. The optics require the presence of pronounced crystalline cones (CCs) and a clear zone. **(C)** Compound eye development is best understood in *D. melanogaster*, in which specific cell types are sequentially recruited from a precursor epithelium. Top: Diagram of cell fate specification and differentiation in the *Drosophila* compound eye. Bottom: The four SCs within each ommatidium show Cut immunoreactivity (green) in the larval, pupal, and adult stages. For better orientation, counterstained tissue is illustrated in magenta: ELAV in larvae, E-cadherin in pupae, and drosocrystallin (lenses) in adults.

Consequently, from a strictly optical perspective, apposition organization allows each lens to project a tiny, inverted image onto the underlying PR array. Therefore, neighboring units function relatively independently. The second compound eye type is the more derived superposition eye as exemplified by the Sunburst Diving Beetle *Thermonectus marmoratus* (Figure 1B). In this eye type many lenses are precisely organized to allow the synergistic projection of images onto the underlying PR array (Nilsson, 1989), which increases light sensitivity (Warrant, 1999). To facilitate optical pooling, this organization requires a clear zone between the optical components and a more distally placed rhabdom layer. Because large parts of the eye must work together, even small changes in the arrangement can lead to optical deficiencies. Despite these functional and structural differences, the cellular organization of ommatidia is relatively conserved, with few differences among arthropods (Paulus, 1979).

Building on genetic studies in *D. melanogaster*, the development of insect compound eyes has been shown to share similar patterns, irrespective of eye type (Friedrich, 2003). For example, PRs develop first from a precursor epithelium, followed by accessory cell development and ultimately lens secretion, pigment cell differentiation, and photoreceptor morphogenesis (Buschbeck and Friedrich, 2008). This process is best understood in the compound eyes of *D. melanogaster*. Due to their precise crystalline organization, and ease of genetic manipulation, the development of these eyes has become a key model for studying organogenesis and tissue patterning. Forming from an undifferentiated neuro-epithelial imaginal disc of a late third instar larva, an eye develops that has ~800 ommatidia, each containing eight PRs, four Semper (cone) cells (SCs), and two primary pigment cells (PPCs), all surrounded by pigmented epithelium-like tissue (composed of higher-order pigment cells) that optically isolates individual ommatidia (Figure 1C) (Charlton-Perkins and Cook, 2010).

At the molecular level, several genes, including *pax6*, have been identified as being part of an ancestrally conserved gene network

(the retinal determination network, RDGN) that underlies early eye development (Gehring, 2001; Kumar and Moses, 2001; Mishra and Sprecher, 2020). Although some differences have been observed in the expression of these genes among individuals with different eye types (Samadi et al., 2015; Schomburg et al., 2015; Klann and Seaver, 2019; Gainett et al., 2020), the genes in the RDGN are important for specifying the early developing cells of ommatidia and are known to be well conserved among some species (Gehring, 2001; Kumar, 2001; Hsiung and Moses, 2002; Mishra and Sprecher, 2020). A few studies have highlighted the nuances of how conserved expression patterns affect early eye development in different species (Yang et al., 2009a; Yang et al., 2009b; Perry et al., 2016). However, relatively little is known about how conserved genes that can influence later eye development processes, such as the delineation of ommatidia as discrete units, act in different compound eyes. One gene of interest is the homeodomain transcription factor *cut*, which in *D. melanogaster* ommatidia is known for its specific expression in SCs.

SCs are recruited immediately after PRs through a combination of extrinsic signaling factors and intrinsic transcription factors (Charlton-Perkins et al., 2021). Two such factors that are essential to the coordination of these events are Pax2 and Prospero, which cooperatively specify SCs and later independently control PR structure and function. SCs are in close proximity to PRs and are a key component of ommatidia (Figure 1B) with multiple roles, including recruiting PPCs, patterning the interommatidial cells, secreting the lens and pseudocone, and serving structural and functional support roles for retinal photoreceptors (Waddington and Perry, 1960; Cagan and Ready, 1989; Querenet et al., 2015; Stahl et al., 2017b; Charlton-Perkins et al., 2017; Charlton-Perkins et al., 2021). Their organization into a quartet is an evolutionarily conserved feature of arthropod compound eyes (Richter, 2002; Schwentner et al., 2018; Scholtz et al., 2019). In *D. melanogaster*, the transcriptional regulation of SC fate determination is relatively well understood (Cagan and Ready, 1989; Kumar, 2012; Morrison et al., 2018; Charlton-Perkins et al., 2021) and their differentiation follows closely that of PRs. As they secrete part of the corneal lens and the pseudocone during the second half of development, SCs are important candidates for influencing the optics of developing eyes. Evidence for their glial nature stems from physiology, which demonstrates ionic and metabolic support for PRs, and from their molecular profile (Cagan and Ready, 1989; Charlton-Perkins et al., 2017). SCs also express important conserved transcription factors, such as Pax2, which is upstream of Cut (Fu and Noll, 1997; Charlton-Perkins et al., 2021).

Cut is a particularly interesting transcription factor because it is a known marker of SCs within *D. melanogaster* ommatidia (Fu and Noll, 1997; Charlton-Perkins et al., 2011). It has been established that the SC-specific expression of Cut lasts throughout the life of *D. melanogaster* (Figure 1C) (Charlton-Perkins et al., 2011). In SCs, Cut has been shown to partner with other transcription factors like Lozenge and Groucho to repress the expression of developmentally relevant genes like *deadpan* (Canon and Banerjee, 2003). Outside eyes, Cut is generally known for its developmental role in cell growth regulation and cell type differentiation (Nepveu, 2001). In *D. melanogaster*, it controls early cell fate decisions in most embryonic tissues, including the nervous system (Blochlinger et al., 1993). In external sensory organs, *cut* specifically belongs to a network of genes that are essential for the accurate maturation of specific sensory neurons and perineurial glia (Blochlinger et al., 1991; Bauke et al., 2015; Corty et al., 2016). Additionally, Cut prevents chordotonal cell fates in these external sensory organs (Blochlinger et al., 1991) and is required for the accurate morphogenesis of other sensory organs such as mechanosensory bristles and auditory organs in *D. melanogaster* (Hardiman et al., 2002; Ebacher et al., 2007) and *Tribolium castaneum* (Klann et al., 2021). Despite the known important developmental roles in the *D. melanogaster* nervous system, the function of Cut within SCs remains largely unexplored.

To investigate the potential contribution of Cut in SCs to the development of two very different compound eye types (apposition optics in *D. melanogaster* and superposition optics in *T. marmoratus*), we first established that Cut expression is conserved in SCs. We then conducted a comparative loss-of-function study and found remarkably similar knockdown phenotypes; this is consistent with the idea that a versatile shared developmental pathway underlies functionally different eye types.

Materials and methods

Animal husbandry and knockdowns

Drosophila melanogaster

All flies were reared on standard cornmeal (made in-house) under a 12 h light–dark cycle at 27°C in 60%–70% humidity. Unless stated otherwise, adult flies were age controlled to 3 days old post-eclosion at the time of experimentation. For knockdown lines, the following alleles from the Bloomington *Drosophila* Stock Center (BDSC) and the Vienna *Drosophila* Resource Center (VDRC) were used: UAS-*cut*RNAi (GD4138)^{VDRC1237}, UAS-*cut*RNAi (TRIP V20 {HMS00924}attP2)$^{(BDSC\ 33967)}$, UAS-*gfp*RNAi$^{(BDSC\ 9330)}$, and UAS-mcherryRNAi (kindly provided by Dr. Vikki Weake, Purdue University (Stegeman et al., 2018). We used *pros*^{PSG}-*GAL4* (*Charlton-Perkins et al., 2017*) to drive the UAS-*ct*^{RNAi} target in prospero-positive R7 and SCs. Flies with the following genotypes were used to generate *cut* knockdowns: 1) *yw*^{67}; *pros*^{PSG}-GAL4/*CyO*; UAS-*cut*RNAi/UAS-*cut*RNAi (*ct*^{GD}), 2) *yw*^{67}; *pros*^{PSG}-GAL4/*pros*^{PSG}-GAL4; UAS-*cut*RNAi/UAS-*cut*RNAi (*ct*^{v20}), 3) *yw*^{67}; *pros*^{PSG}-GAL4/*pros*^{PSG}-GAL4; UAS-*gfp*RNAi/UAS-*gfp*RNAi (control flies used in all experiments); and 4) *yw*^{67}; *pros*^{PSG}-GAL4/*pros*^{PSG}-GAL4; UAS-mcherryRNAi/UAS-mcherryRNAi (a second control line for electrophysiology) (Figure 7; Supplementary Figure S3).

Thermonectus marmoratus

The beetles used in this study were separated from our lab-grown colony at the third instar stage. Each larva was allowed to develop into an adult beetle in an individual pupation chamber filled with sand. All animals were reared under a 14 h light–10 h dark cycle at 25°C. Unless stated otherwise, adult beetles were ~1 day old post-eclosion at the time of experimentation. To generate dsRNA against *cut*, we first identified the mRNA transcript of *cut* based on the three Cut domains and a homeobox domain (Supplementary Figure S2; Supplementary Table S1) from transcriptomics (Stahl et al., 2017a). To generate the probe, a 512 bp long unique region (outside the Cut and homeobox domains) was identified and amplified (see Supplementary Table S1; Supplementary

Figure S2 for primers) from whole tissue cDNA. This amplicon was used for dsRNA synthesis as described in (Rathore et al., 2020). Then, 100 ng of *cut* dsRNA was injected in late-stage third instar larvae to ensure *cut* knockdown early during compound eye development (which is initiated during the pre-pupation stages in *T. marmoratus* larvae; personal observation).

Immunohistochemistry

Drosophila melanogaster

Larval, pupal, and adult eyes were processed as described (Charlton-Perkins et al., 2011) and stained with mCut (DHSB, 1:20), Elav (DHSB, 1:50), DCAD2 (E-cadherin; DHSB, 1:50), and drosocrystallin (kindly gifted by H. Matsumoto; rbCry 1:100; Figure 1). The samples were imaged using a Nikon A1R multiphoton confocal microscope, and image processing was performed using NIS-Elements (Nikon) and Photoshop CC (Adobe). For Cut and N-cadherin staining, the pupal eye discs were dissected at ~ 37% development as outlined in Tea et al., 2014. In brief, tissue was fixed in 4% formaldehyde diluted in dissection solution for 20 min at RT. Post fixation, the eye discs were washed three times in PBT (PBS with 0.3% Tween 20). Then, 10% normal goat serum (NGS) in PBT was used to block the eye discs at RT. The eye discs were incubated in primary antibodies (anti-Cut 1:50 (DSHB) and anti-N-cadherin 1:50 (DSHB) in PBT) at 4°C for ~40 h. Anti-mouse Alexa Fluor 488 and anti-rabbit Alexa Fluor 488 were used as secondary antibodies at 1:500 for 2 h at RT. Subsequently, the eye discs were washed in PBT, the nuclei counterstained with DAPI, and after additional washing, mounted in Fluoromount (Fisher Scientific). Z-stacks were acquired using a Leica Stellaris eight confocal microscope with a ×40 objective at a resolution of 1,024 × 1,024 pixels and a pixel size of 0.047 µm.

Thermonectus marmoratus

Pupal eyes (at day 2 APF) were dissected and processed as described for *D. melanogaster* eyes, except that the tissue was counterstained with phalloidin (Alexa Fluor 647, Thermo Fisher) instead of anti-N-cadherin (due to a lack of cross-reactivity). The anti-Cut antibody previously has been successfully used in beetles (Burns et al., 2012; Miguel et al., 2016). Z-stacks were acquired using a Zeiss LSM 710, AxioObserver confocal microscope with a ×40 objective at a resolution of 512 × 512 pixels and a pixel size of 0.11 µm. All images were processed using ImageJ, and the brightness and contrast were adjusted using Adobe Photoshop 2022.

Confirmation of cut knockdown

Cut immunostaining also was used to qualitatively confirm the success of our knockdowns. For this we analyzed confocal images of control and knockdown individuals, that were taken with identical imaging settings. For each individual we averaged the gray value from the center of 40 (for the smaller *D. melanogaster* or 160 (for the larger *T. marmoratus*) Semper cells and contrasted them to the average of 20 background points for normalization (Supplementary Figures S1C, D). This was possible for *T. marmoratus* as well as the ct^{GD} *D. melanogaster* line, however knockdown was so efficient in the ct^{V20} line that cells could not be well enough recognized for this analysis.

Cryosectioning and phalloidin staining

Control and *cut* knockdown fly and beetle heads were fixed in 4% formaldehyde overnight at 4°C. These tissues were washed three times with PBS and then cryoprotected overnight at 4°C in sucrose solutions of increasing concentrations (20%, 40%, and 60%). The samples were mounted in Neg50, flash frozen in liquid nitrogen, and cryosectioned at ~18 µm (Leica CM 1850). The sections were dried, rinsed in PBS, and stained with Phalloidin (following manufacturer's instruction) and mounted with Fluoromount containing DAPI (Thermo Fisher). Z-stacks for *D. melanogaster* samples were obtained at a resolution of 1,024 × 1,024 pixels using a Leica Stellaris eight confocal microscope with a ×40 objective. *T. marmoratus* samples were imaged using a Zeiss LSM 710, AxioObserver confocal microscope with a ×40 objective. The entire eye was tile scanned with a constant pixel size of 0.69 µm. All images were processed using ImageJ, and brightness and contrast were adjusted using Adobe Photoshop 2022.

Differential interference contrast (DIC) microscopy and optical assessments

D. melanogaster and *T. marmoratus* heads for all groups were dissected in 100% and 50%, respectively, insect ringer (O'Shea and Adams, 1981) to maintain an appropriate osmotic environment and prevent the lens proteins from denaturing. Isolated lenses were suspended in corresponding insect ringer dilutions between coverslips to allow imaging of the undersurfaces of the lenses *via* DIC microscopy (Nomarski Optics, Olympus BX51 microscope with a ×40 Uplan objective) as well as assessment of the optical quality of the lenses by visualizing the images produced by the lens array. The so-called "hanging drop method" follows protocols that were originally developed by (Homann, 1924) and since then commonly used in investigations of insect optics (Wilson, 1978; Buschbeck et al., 1999; Warrant et al., 2006; Stowasser et al., 2010). A representation of a 2 mm grating was projected through the lenses and pictures were taken of the resulting arrays of images that were focused by the lens arrays. All pictures were obtained using a microscope camera (Qimaging, Retiga 2000R) and the brightness and contrast were adjusted using Adobe Photoshop 2022.

Electron microscopy (EM)

Transmission EM (TEM)

D. melanogaster and *T. marmoratus* heads were dissected, fixed, and prepared for sectioning using standard protocols (Wolff, 2011) modified in the lab (Stowasser and Buschbeck, 2012). Images were acquired using a transmission electron microscope (JOEL JEM-1230 and Hitachi H-7650). The brightness and contrast were adjusted using Adobe Photoshop 2022.

Scanning EM (SEM)

D. melanogaster and *T. marmoratus* heads were dissected, dried at −20°C, and mounted on stubs with adhesive carbon pads (Electron Microscopy Sciences). The stubs were sputter coated with gold and imaged using a scanning electron microscope (FEI Apreo LV-SEM). The brightness and contrast were adjusted using Adobe Photoshop 2022.

Extracellular electroretinogram (ERG) measurements and statistical analysis

The genetic background in both groups resulted in increased variability in eye color. Since eye color influences the strength of ERG responses, the tested flies were visually color matched. As the two species have different spectral sensitivity peaks (Maksimovic et al., 2011; Sharkey et al., 2020), testing was carried out using a 490 nm light source for *D. melanogaster* and a 525 nm light source for *T. marmoratus*. The first test was used to assess the range of light intensities that led to PR responses (V–logI curves). This test consisted of a series of three 1 s long light flashes of increasing intensities, with each flash being ~10 s apart to allow PR recovery. The second test was used to identify whether the PRs could sustain a response to a train of consecutive light flashes (extended sequence). This test consisted of a series of 150 light flashes at a single light intensity that was within the linear range of PR responses.

For *D. melanogaster* controls (*gfp*RNAi and *mcherry*RNAi) and *cut*RNAi (ct^{GD} and ct^{V20}), flies were prepared and used for ERG measurements as previously described (Charlton-Perkins et al., 2017). A V–logI curve was established for each group using the following light intensities (photons/cm^2/s): 4.28×10^{10}, 8.15×10^{10}, 2.78×10^{11}, 7.20×10^{11}, 1.75×10^{12}, 5.42×10^{12}, 1.04×10^{13}, 5.53×10^{13}, and 1.07×10^{14}. To ensure steady recording, each series started with a pre-pulse of full light intensity. The extended sequence was administered at 7.20×10^{11} photons/cm^2/s (the light intensity at which the PRs were ~50% saturated), with light and interval durations of 300 ms.

For *T. marmoratus* controls and *cut*RNAi, beetles were anesthetized using carbon dioxide. These beetles were secured on a glass slide with dental wax and then allowed to dark adapt for 10 min before establishing V–logI curves using the following light intensities (photons/cm^2/s): 5.00×10^{11}, 1.90×10^{12}, 5.00×10^{12}, 1.00×10^{13}, 2.20×10^{13}, 5.50×10^{13}, 1.14×10^{14}, 2.25×10^{14}, 3.90×10^{14}, and 1.07×10^{14}. The recording stability was verified through a high intensity pre-pulse. The beetles were then allowed to dark adapt for 10 min before the extended sequence test was performed at 10^{13} photons/cm^2/s (the light intensity at which the PRs were ~50% saturated). As for flies, each light flash had a duration of 300 ms, however stimulus intervals were increased to 500 ms to allow adequate PR recovery.

All the data were analyzed with a custom-made MATLAB code (Riazuddin et al., 2012; Charlton-Perkins et al., 2017). As some groups didn't show a normal distribution according to the Shapiro-Wilks test, we used Wilcoxon's rank sum test for all intergroup comparisons (in both species). All graphs were plotted, and statistical tests were calculated in R (version 4.0.3, packages Dplyr, tidyr, and ggplot2).

Results

Cut expression is conserved within the four SCs of *Drosophila melanogaster* and *Thermonectus marmoratus* compound eyes and can be successfully knocked down in both species

In *D. melanogaster,* Cut is expressed in the four SCs of each ommatidium and the interommatidial mechanosensory bristle (Figure 2A; Supplementary Figure S1A) (Blochlinger et al., 1990). Our immunohistochemical investigation using an antibody which was made against the *D. melanogaster* Cut, found it also expressed in the SCs of *T. marmoratus*, suggesting a high level of protein conservation between the two species (Figure 2B). N-cadherin and DAPI (for *D. melanogaster*) or actin and DAPI (for *T. marmoratus*) were used to confirm the position of the SC cell bodies distal to the developing PRs and rhabdoms. These similarities led us to hypothesize a conserved functional role for this transcription factor between these two eye types. To test for such conserved roles, we used a loss-of-function approach, applying a Semper cell-restricted knockdown in *D. melanogaster* (Charlton-Perkins et al., 2017) and a generalized dsRNA injection in late stage *T. marmoratus* larvae (Rathore et al., 2020).

To confirm the SC-restricted knockdown in *D. melanogaster*, we analyzed whole mounts of 37% developed pupal retina (which is prior to lens formation) in two different *cut*RNAi lines (ct^{GD} and ct^{V20}) and compared them to a control line (*gfp*-RNAi). We found that SC-directed knockdowns reduced Cut expression either partially (ct^{GD}; $n = 14$; Supplementary Figure S1C) or to an undetectable level (ct^{V20}; $n = 14$, Figure 2A) when compared to controls ($n = 15$). This difference could be due to the driver being heterozygous in ct^{GD} flies and homozygous in ct^{V20} flies, or to differences in knock-down efficiencies between these two lines. To verify that *cut* knockdown was restricted to SCs, we also imaged Cut-expressing interommatidial bristle cells located proximal to the SCs. As expected, Cut expression was unaffected in these cells in all three fly lines (Supplementary Figure S1A).

To ensure a comparable stage and preparation for *T. marmoratus*, we injected *cut* dsRNA (Supplementary Figure S2) in late third instar larvae, and used the cross-reacting Cut antibody to detect expression in early developing whole pupal retina. Cut expression was not detectable in any developing ommatidial cell type except for SCs. Consistent with previous findings (Rathore et al., 2020), we found knockdowns in *T. marmoratus* to be highly successful (Supplementary Figure S1D), with 10 of 12 injected individuals showing reduced Cut expression when compared to controls ($n = 8$). However, complete *cut* knockdown was rare, likely because the individuals with the highest knockdown died during early development. This is expected due to *cut's* vital role in the development of multiple organ systems in insects (Bauke et al., 2015; Corty et al., 2016; Klann et al., 2021). Accordingly, ~53% of the *cut* dsRNA injected individuals died, as opposed to only 27% of the controls. Although the SCs of control individuals strongly expressed Cut, the *cut* dsRNA-injected individuals exhibited SCs with varying, but greatly reduced Cut expression (Figure 2B).

Although the nature of the knockdown differs in the two species, in both cases, treatments were aimed at detecting SC-driven effects within the ommatidial array. We would like to note that this approach led to differential *cut* knockdown in the neuropils between the two species, with *T. marmoratus cut* also being knocked down in other Cut-positive cells in the visual system (e.g., subretinal glia in the lamina), which could lead to additional developmental or neurophysiological phenotypes on photoreceptors in *T. marmoratus* not detected in *D. melanogaster.*

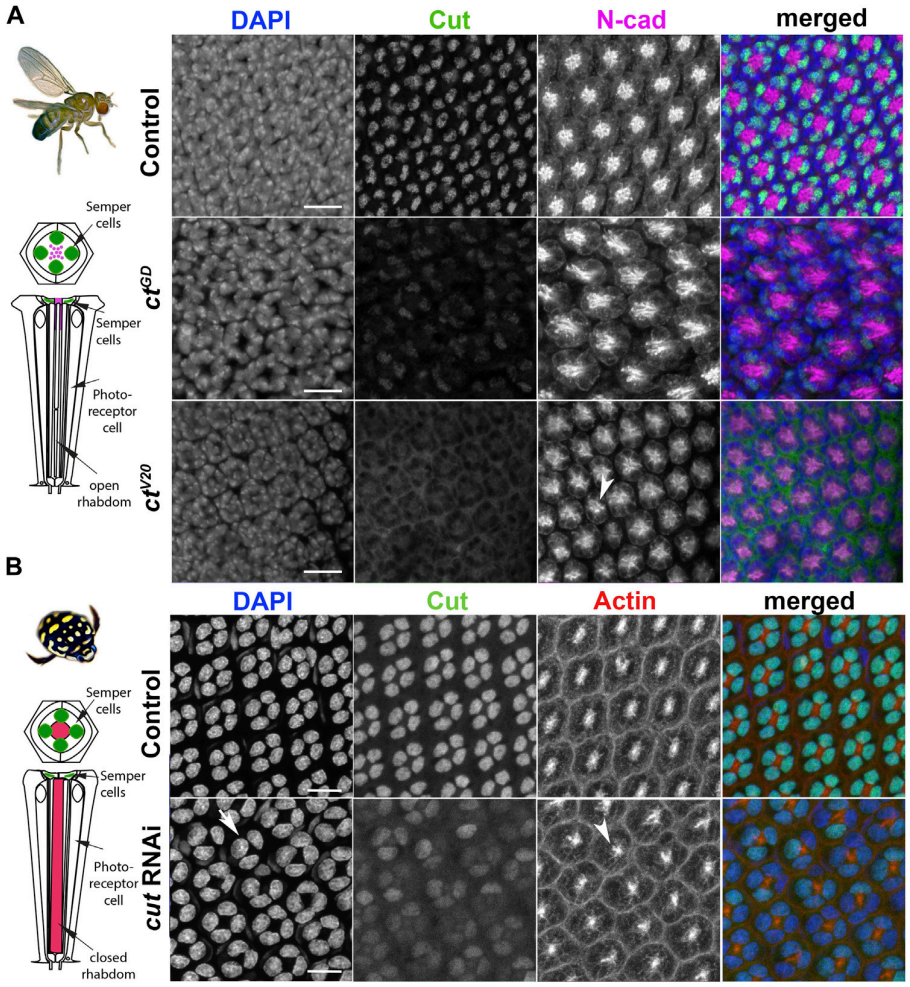

FIGURE 2
Cut expression and RNAi-driven knockdown in *D. melanogaster* and *T. marmoratus* compound eyes. **(A)**. In *D. melanogaster*, a quartet of Cut-positive Semper cells (green) are situated within the distal-most portion of developing ommatidia (at ~37% pupal development). DAPI and N-cadherin counterstaining are used to identify the correct layer within the eye. As illustrated in representative images, efficient *cut* knockdown is achieved by two different SC-directed RNAis, with overlapping phenotypes consisting of an irregular ommatidial array. Incidences of laterally displaced rhabdoms are indicated *via* N-cadherin staining (arrowhead). **(B)**. In *T. marmoratus*, at a comparable developmental stage, four Cut-positive SCs are similarly organized near the distal margin of each ommatidium. At this stage, the closed rhabdom (red; confirmed by actin staining) still resides in close proximity to the SCs. The nuclear localization of Cut is confirmed by complete overlap with DAPI. *cut*RNAi treated individuals show a strong but incomplete reduction of Cut, with irregularities in the ommatidial array. In some instances at this level, only a triad of Cut-positive nuclei are visible (arrow), and rhabdoms appear to be laterally displaced (arrowhead). Scale bars = 10 μm.

Cut in SCs regulates precise ommatidial patterning during the development of different compound eye types

To investigate whether *cut* knockdowns affect the ommatidial organization during development, we examined pupal retinae for patterning defects. In *D. melanogaster*, N-cadherin allowed visualization of the position of the apical membranes of SCs and their relative position to PRs (Hayashi and Carthew, 2004). For both knockdown lines, we found visible organizational changes in these cell types as well as irregularities in the placement of ommatidia (Figure 2A; Supplementary Figure S1B). Typically, at ~40% after puparium formation (APF), SCs are expected to be fully differentiated and organized in a characteristic tetrad, with the inner junctions forming an "H"-like pattern (see (Fu and Noll, 1997; Charlton-Perkins et al., 2021) and control in Supplementary Figure S1B). In contrast, the rhabdomeres in PRs are located within the center of each ommatidium and are expected to elongate toward the basement membrane (Longley and Ready, 1995). In both of the *ct* knockdown lines, the typical "H" shape (indicative of a tetrad of SCs) failed to develop. Instead, an irregular pattern emerged with several instances of triads (Supplementary Figure 1B). In parallel, the *cut*RNAi of the developing *T. marmoratus* pupal retina also showed irregularities and instances of SC triads (Figure 2B). Although not verifiable with the N-cadherin antibody due to a lack of cross-reactivity, this phenomenon was clearly apparent with DAPI. The

presence of triads in both species suggests that only three of the four SCs in these ommatidia developed properly, with one of the cells likely either absent or radically displaced.

Additionally, for *D. melanogaster*, control PRs had (as expected) centrally located rhabdomeres, whereas both *ct* knockdown lines showed displaced rhabdomere organization. Deficiencies included the dislocation of rhabdomeres from the central position of the ommatidium (Figure 2A). In parallel, based on actin counterstaining of the actin-rich rhabdom structures, several of the fused rhabdoms in the *T. marmoratus cut*RNAi individuals also lost precise alignment at the center of the ommatidia relative to controls (Figure 2B). Taken together, these observations show that *cut* knockdown in compound eyes results in complimentary developmental organizational deficiencies in both SCs and PRs. To investigate the functional implications of these developmental defects in adult compound eyes, we focused on the three known major functions of SCs: lens formation, PR and rhabdom morphogenesis, and PR functional support.

Effects of *cut* knockdowns on PR placement and rhabdom morphogenesis

Lens secretion begins at ~50% pupal development of *D. melanogaster* retina, and the role of SCs in this process has been well documented (Cagan and Ready, 1989; Charlton-Perkins and Cook, 2010). Considering our findings that Cut disrupts accurate SC patterning, we next asked if these SC defects could lead to structural and functional defects in adult compound eye corneal lenses. To address this question, we first assessed the outer lens surfaces at an ultrastructural level. In both *D. melanogaster* (Figures 3A–F) and *T. marmoratus* (Figures 3G–K), knockdown individuals showed visible defects in lens morphology, shape, and organization when compared to controls.

In *D. melanogaster*, in contrast to the precisely organized lenses of controls (n = 9; Figures 3A, D), both *cut* knockdown lines (ct^{GD}: n = 10, ct^{V20}: n = 14) showed major defects, including a rough eye appearance and variation among lenses (Figures 3B, C). In both lines, we observed instances of fusion of neighboring units and flatter lenses, some of which had visible indentations on the outer lens surface (Figures 3E, F), a phenotype previously referred to as the "blueberry phenotype" (Higashijima et al., 1992). The latter phenomenon was particularly prominent in the ct^{V20} line. The positions of the indentations were often asymmetric, possibly relating to differential contributions by different SCs.

Adult *T. marmoratus* compound eyes tended to have a smooth surface, which appeared similar in control and *cut*RNAi individuals at low resolution (Figures 3G, H). However, the RNAi individuals (n = 6) showed an increase in dimple-like developmental defects on the outer eye surface (~80% of individuals) when compared to controls (~20%; n = 7; Figure 3I). Higher resolution images revealed that unlike the highly regular and seamlessly connected lens arrays of controls (Figure 3J), *cut*RNAi individuals generally had irregular lens shapes and pronounced ommatidial boundaries.

To assess lenses from a functional perspective, we isolated lens arrays and mounted them onto a droplet of insect ringer (hanging drop method). This approach allowed examination of the back surfaces of the lenses as well as the visualization of the corresponding images formed by the isolated lens arrays. In both species, control individuals (n = 6 for *D. melanogaster* and 10 for *T. marmoratus*) exhibited smooth lens surfaces (Figures 4A–D), and the images produced by the lens arrays were regularly spaced with uniform image magnification (Figures 4A′–D′). In contrast, in *D. melanogaster ct* knockdown lines, the aforementioned lens deficits were also visible from the back surface (n = 6 for each line; Figures 4B, C). Notably, in ct^{V20} individuals, some lenses appeared necrotic (Iyer et al., 2016), while others showed small indentations. Optically, both lines showed instances where neighboring lenses formed images with irregular placement, focused at different planes, and exhibited variable image magnification (Figure 4B′, C′). For the ct^{V20} line, we also noted that some lenses with holes that entirely failed to form images.

Mirroring the findings from *D. melanogaster*, *cut* dsRNA injected *T. marmoratus* (n = 10) exhibited irregular lens arrays with centrally located indentations on the back surfaces (Figures 4E, F). Many of the lens back surfaces also appeared flatter. Accordingly, the images produced by the lens arrays differed in placement, quality, and image magnification (Figures 4E′, F′). Taken together, these results suggest that Cut is generally required by SCs for accurate lens formation with proper optics in both compound eye types.

Effects of *cut* knockdowns on PR placement and rhabdom morphogenesis

SCs are located in close proximity to PRs, and in *D. melanogaster*, they are known to provide glial support (ionic, metabolic, and structural) to PRs (Charlton-Perkins et al., 2017). The same study also demonstrated that SC-specific *pax2*RNAi results in defective rhabdom morphogenesis. Considering that Cut functions downstream of Pax2 and based on our observed displacements of the developing rhabdoms, *cut* knockdown could also lead to misformed adult rhabdoms.

It is important to note that *D. melanogaster* has open rhabdoms (each consisting of eight rhabdomeres) that extend distally close to the SC bodies (Figures 5A, B), whereas in *T. marmoratus*, closed rhabdoms are separated from the SCs *via* a clear zone (Figures 5E, F). As illustrated by phalloidin staining, despite these structural differences, we found similar knockdown phenotypes in the two species.

In *D. melanogaster*, compared to the pristinely organized rhabdoms of control individuals that traverse the entire length of each ommatidium (n = 10; Figure 5B), the rhabdoms for both ct^{GD} (n = 7) Figure 5C and ct^{V20} (n = 6) Figure 5D knockdown individuals were truncated. Generally, they either failed to reach the basement membrane or were present deep in the eye, either traversing the basement membrane or are seen proximally to it. Similarly, in *T. marmoratus*, controls (n = 7) showed precisely placed PRs with a well-defined clear zone (Figure 5F). However, the retina of *cut*RNAi individuals (n = 7) showed irregular PR placement (including misplaced nuclei), with some PRs extending to and even through the basement membrane (Figure 5G). Additionally, the clear zone in these individuals was less well defined.

At an ultrastructural level, *D. melanogaster* controls (based on two TEM preparations) exhibited the classical trapezoid organization (Longley and Ready, 1995) with seven visible open rhabdomeres (Figures 6A, B). In contrast, individuals from both the ct^{GD} (n = 3) and ct^{V20} (n = 2) lines exhibited parallel deficiencies, such

10.3389/fcell.2023.1104620

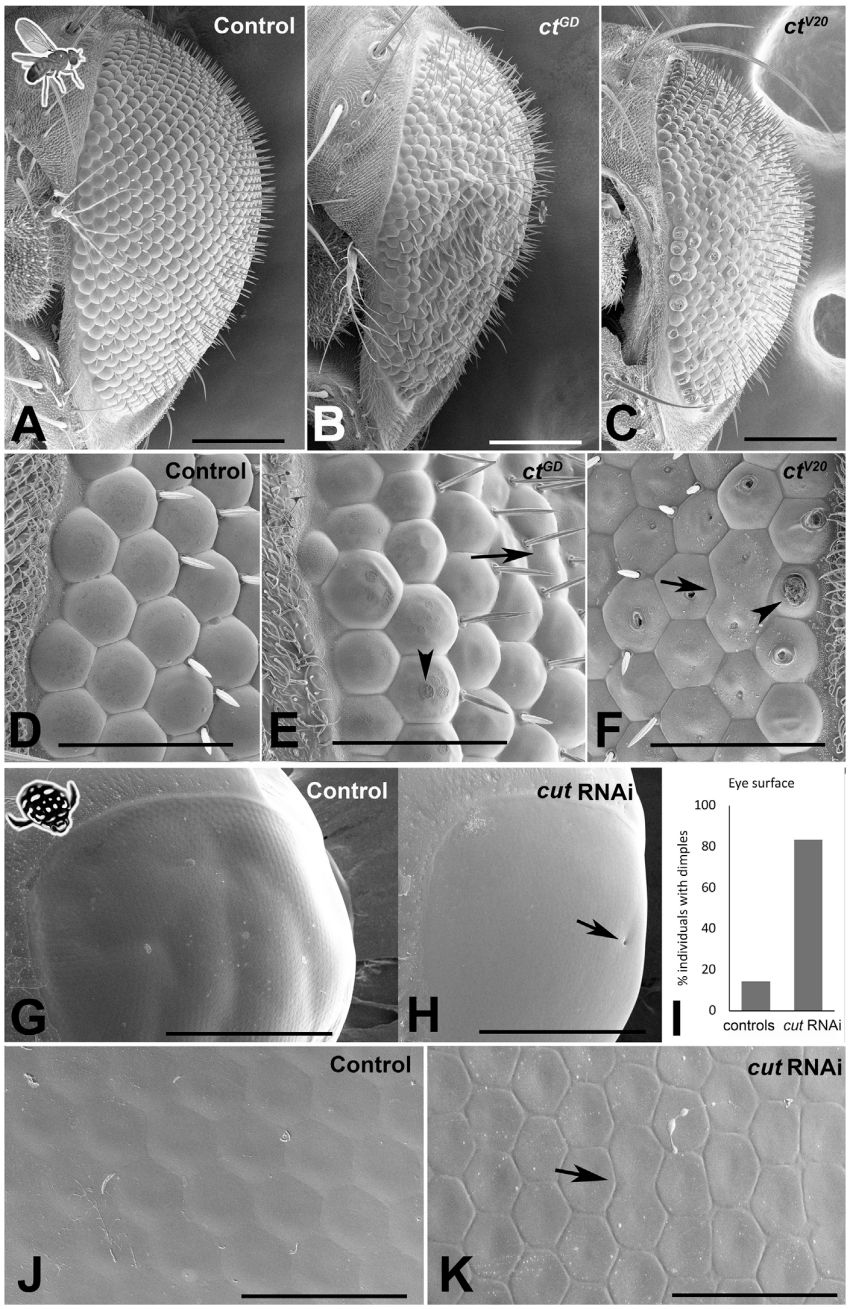

FIGURE 3
Cut knockdown affects lens organization in insect compound eyes. **(A–F)** Scanning electron micrographs of adult *D. melanogaster* compound eyes. Overview of a control individual **(A)** illustrates a typical completely regular ommatidium array, whereas ct^{GD} **(B)** and ct^{V20} **(C)** exhibit major irregularities in ommatidial placement and lens formation. The latter is illustrated in a magnified view of the anterior region of the compound eye. In control individuals **(D)**, lenses appear precisely shaped with properly formed lens surfaces. In ct^{GD} **(E)** and ct^{V20} **(F)**, irregularities exist in ommatidium separation, with some neighboring units fused (arrows). In some instances, the lens surface exhibits deformities typical of the blueberry phenotype (arrowheads), which are particularly pronounced in the ct^{V20} line. **(G–K)** Scanning electron micrographs of adult *T. marmoratus* compound eyes. Overview of a control beetle **(G)** shows an intact eye with a smooth surface. In *cut*RNAi individuals **(H)**, surface dimples (arrow) are more common than in controls **(I)**. A high-resolution image of the anterior region of the compound eye illustrates precise placement and smooth transitions between neighboring ommatidia **(J)**, whereas *cut*RNAi injected individuals show irregularities in ommatidium size and more delineated borders **(K)**. Additionally, some neighboring units are fused (arrow). Scale bars = 100 μm **(A–C)**, 40 μm **(D–F)**, 500 μm **(G, H)**, and 50 μm **(J, K)**.

as irregularly spaced ommatidia (Figures 6C–F), a reduced number of rhabdomeres (Figures 6C–H), split rhabdomeres (Figures 6D, E, G), and fused rhabdomeres (Figure 6H). For *T. marmoratus*, controls showed regularly organized closed rhabdoms, whereas rhabdom abnormalities were observed in *cut* RNAi individuals (Figures 6I, J). The retina of *cut*RNAi individuals showed irregularly placed rhabdoms, with some units being on a different plane within the same array (Figures 6K, N). Additionally, the rhabdoms were frequently incomplete and off center (Figures 6M, O) with instances of split and broken manifestations (Figures 6L, P) and signs of degeneration (Figure 6P). Overall, these results suggest that Cut could function in SCs to direct the proper development of PRs in both compound eye types.

Effects of *cut* knockdowns on PR function

To understand whether morphological defects related to *cut* knockdowns also affected function, we used electroretinograms (ERGs), an extracellular recording technique that measures the response of the PR array to light stimuli (Belusic, 2011; Riazuddin et al., 2012; Charlton-Perkins et al., 2017).

In *D. melanogaster,* we first assessed the dynamic ranges of PR responses to increasing light intensities (Figure 7A) and found relatively normal responses in both knockdown lines (Figure 7B). Figure 7A illustrates the response curves for individuals from both control and *cut*RNAi lines to 490 nm light stimuli of an intermediate light intensity (7.2×10^{11} photons/cm^2/s). As expected from a normal fly ERG, control PR responses were flanked by on and off transients. Although flies from both *cut*RNAi lines had slightly reduced PR responses, there was no statistical difference at two different light intensities (Figure 7C), which may, in part, be due to the high variability in all groups, which may be related to slight differences in eye color. In *T. marmoratus*, all controls had normal PR responses, but dramatic differences existed in *cut*RNAi individuals, which were separated into three categories (Figure 7D): 1) Individuals with normally shaped responses at all light intensities, 2) individuals with normally shaped responses at low light intensities but inverted responses at higher light intensities, and 3) individuals with reversed-polarity responses at all light intensities. To keep the quantitative analysis comparable to controls, only individuals with electronegative responses were incorporated into the statistical analysis. Figure 7E illustrates such normal and reversed potential responses. In some cases, in a train of pulses, only the first response was inverted (Figure 7H). As shown in Figure 7F, even the normal, electronegative responses of *cut*RNAi individuals tended to be lower than those of controls ($n = 15$), with a significant difference at a light intensity of 10^{13} photons ($n = 7$; $p = 0.0015$, Wilcoxon's test) but not at 4×10^{13} ($n = 4$; $p = 0.08$, Wilcoxon's test) (Figure 7G). Note that statistical power was lost at higher light intensities due to smaller sample sizes resulting from an increased occurrences of reversed polarity potentials (5.00×10^{11}, $n = 8$; 1.90×10^{12}, $n = 8$; 5.00×10^{12}, $n = 8$; 1.00×10^{13}, $n = 7$; 2.20×10^{13}, $n = 5$; 5.50×10^{13}, $n = 5$; 1.14×10^{14}, $n = 5$; 2.25×10^{14}, $n = 4$; 3.90×10^{14}, $n = 5$; and 1.07×10^{14}, $n = 4$).

It has previously been demonstrated that certain genetic perturbations can affect the ability of flies to maintain a proper photoresponse throughout a long series of light pulses (Riazuddin et al., 2012). To test if such deficiencies exist in *cut* knockdowns, we exposed flies and beetles to a series of 150 light pulses (extended sequence) (Supplementary Figure S3). To assess differences in the PR potentials at earlier and later time points, the responses were analyzed by grouping the data into 10-point bins. Since some early signal reduction is normal (due to adaptation), we limited our analysis to bins 3–15. No significant differences between these bins were observed in any of the fly lines (Supplementary Figures S3A, B, $p = 0.97$, 0.97, 0.44, and 0.58, Wilcoxon's test) or the controls and *cut* RNAi beetles (Supplementary Figures S3C, D, $p = 0.29$ and 0.28, Wilcoxon's test). Consistent with our analysis at different light intensities (Figure 7G), *cut* RNAi beetles showed slightly lower responses than the controls. Apart from some inverted responses in *cut* RNAi injected beetles (Figures 7E–H), our ERG analysis didn't reveal any major differences between the controls and knockdowns in either compound eye type.

Discussion

We employed a comparative approach to test how Cut in SCs contributes to the development of two different compound eye types in insects. Our data support that this generally deeply conserved homeodomain transcription factor (CUX in vertebrates) is part of a deeply conserved gene network that is essential for proper eye development. The observed parallels are especially exciting because they are consistent with the idea that a common developmental pattern underlies diverse eye organizations (Lavin et al., 2022), and adds to a list of already known relatively well established deeply conserved genes, such as those of the RDGN (Gehring, 2001; Kumar and Moses, 2001; Mishra and Sprecher, 2020).

Importance of *cut* in SCs for precisely patterned compound eyes

Our comparative study suggests that if *cut* is knocked down, the crystalline precision of the eye is disrupted relatively early in development, irrespective of the compound eye type. The key to this phenomenon likely lies in the central role of SCs for ommatidium development and of Cut for proper patterning of SCs.

During eye development, SCs undergo dramatic changes in organization (Cagan and Ready, 1989) and play important roles in recruiting later-developing PPCs (Nagaraj and Banerjee, 2007) and regulating the orientation of developing PRs. The specific patterning steps of SCs likely include a combination of forces driven by the actomyosin cytoskeleton, cell adhesion (Cadherins and Nephrins), endocytosis, and Notch signaling (Chan et al., 2017; Blackie et al., 2020; Blackie et al., 2021; Charlton-Perkins et al., 2021). As Cut expression is detectable shortly after SC specification (Blochlinger et al., 1990; Canon and Banerjee, 2003; Charlton-Perkins et al., 2011), it is well positioned to contribute to the regulation of these patterning events. Consistent with this possibility, in both species, *cut* knockdowns lead to defects in cell

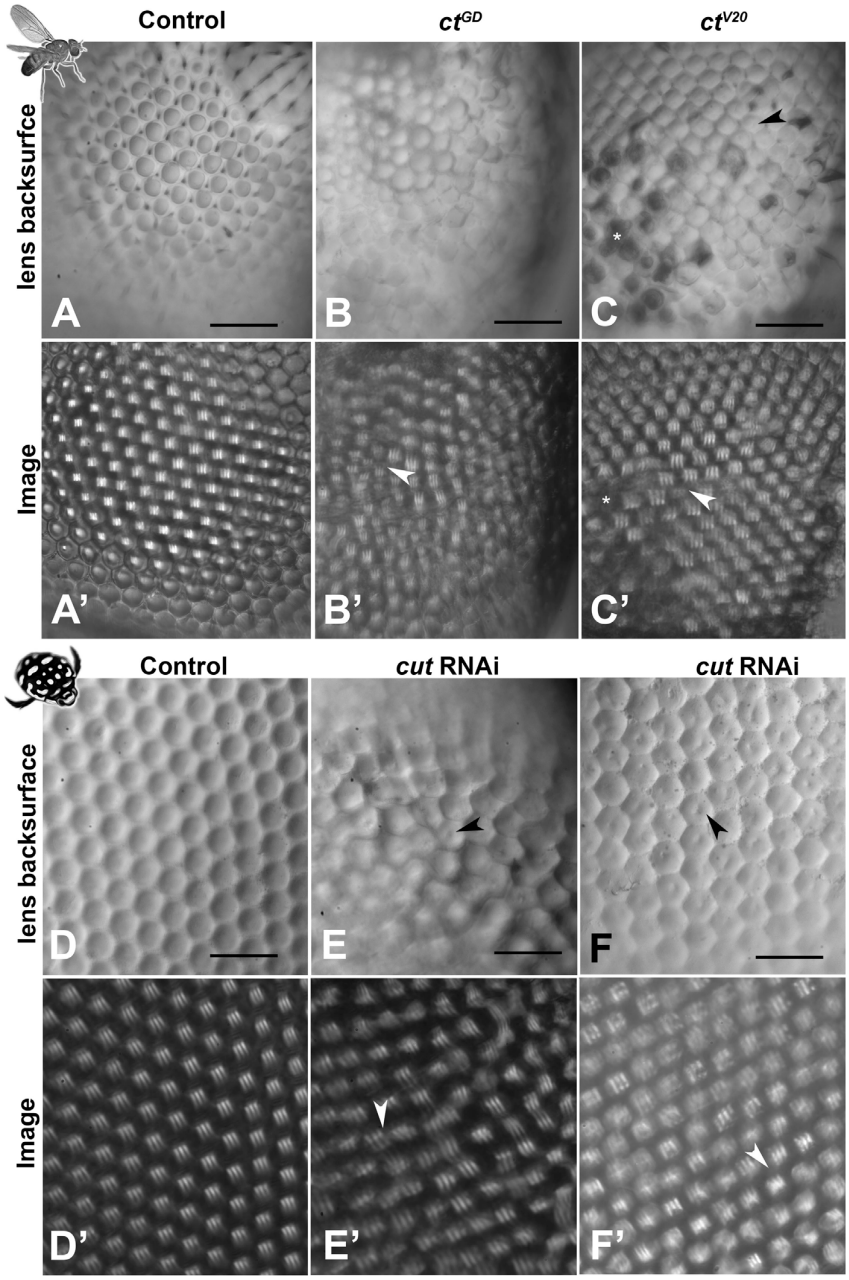

FIGURE 4
Morphological lens defects lead to profound optical deficits. Isolated lens arrays were used to visualize the back surfaces of lenses **(A–F)** and images of an object with three stripes were then produced by these lens arrays **(A'–F')**. In *D. melanogaster*, control lenses have smooth and accurately formed back surfaces **(A)** that lead to regularly spaced and equally sized images with a uniform focal plane across the lens array **(A')**. In contrast, the lenses of the *cut* knockdown lines show visible defects in morphology **(B, C)** and optics, with images that vary in placement, image magnification (arrowheads), focal plane, and blurriness **(B', C')**. For ct^{V20}, several lenses show dimple-like indentations on the back surfaces (arrowhead) and other lenses appear dark and necrotic **(C)**. Such necrotic lenses (exemplified by the cluster marked with *) lead to gaps in the resulting image array * in **(C')**. In *T. marmoratus*, a similar pattern is observed, with controls having smooth and even lens back surfaces **(D)** that result in pristine regular image arrays **(D')**. In contrast, *cut*RNAi individuals exhibit lens irregularities **(E)** that lead to irregularities in the corresponding lens array **(E')**, including greatly displaced images (arrowhead). Lens back surfaces frequently show dimple-like lens indentations arrowheads in **(E, F)**, which are also present in individuals with fewer irregularities in lens placement **(F)**. Even in this morphologically less severe phenotype, major deficiencies in the lens array optics occur, resulting in many blurry images and some differently sized images (arrowhead) **(F')**. Scale bars = 50 μm.

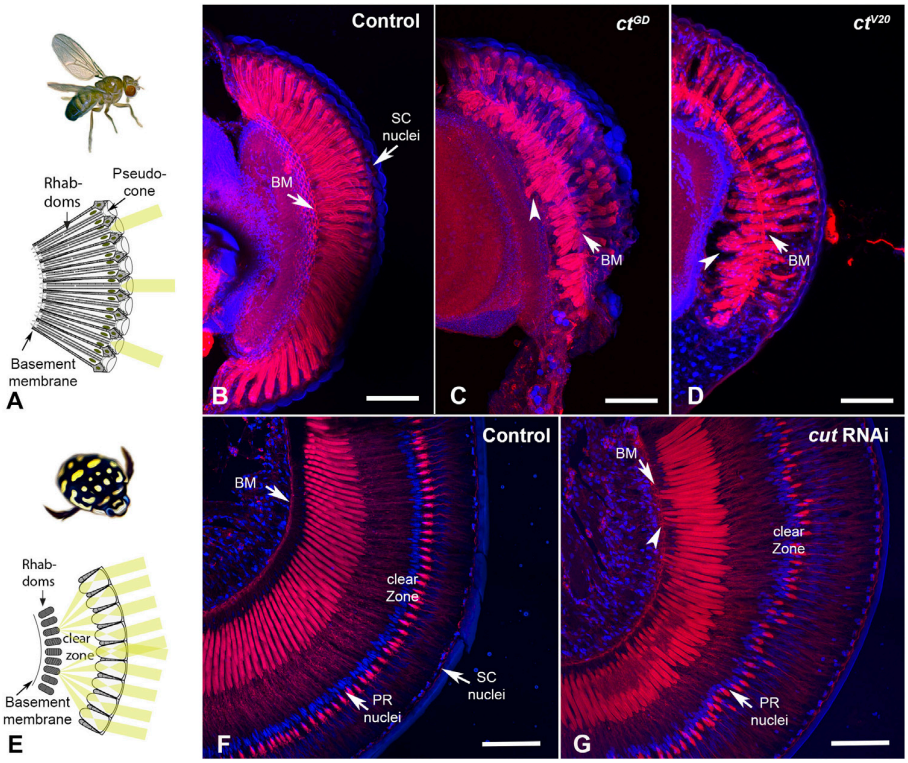

FIGURE 5
Cut knockdown leads to rhabdom misplacement in both eye types. **(A)**. In *D. melanogaster*, rhabdoms typically extend along the majority of the ommatidia, from close to the pseudocone to the basement membrane. **(B)**. Rhabdoms, visualized with phalloidin, appear well developed and regular in control individuals. In ct^{GD} **(C)** and ct^{V20} **(D)** individuals, rhabdoms appear truncated and frequently misplaced, with many extending well below the basement membrane (arrowheads). **(E)**. In *T. marmoratus,* rhabdoms are situated much deeper in the eye to make room for a clear zone, which is necessary to allow many lenses to contribute to the image formed at the distal end of the PRs. **(F)**. Phalloidin staining in control individuals illustrates precisely aligned rhabdoms that extend from below the clear zone to well above the basement membrane (BM). PR nuclei are aligned precisely along a concentric circle between the rhabdoms and lenses. **(G)**. In *cut*RNAi individuals, PR placement is less regular, at the levels of both PR nuclei and rhabdoms. As in *D. melanogaster*, rhabdoms are displaced toward the basement membrane and occasionally traverse it (arrowhead). Scale bars = 50 μm **(B–D)** and 100 μm **(F, G)**.

placement, including the presence of triads or displaced tetrads in the SC layer (Supplementary Figure S1B) and the lateral displacement of adjacent PRs (Figure 2A). Interestingly, these defects are reminiscent of those observed in the developing *D. melanogaster* mutant pupal retina for Pax2, Hibris, Roughest, Mastermind (a Notch signaling inhibitor), and Wingless (Grillo-Hill and Wolff, 2009; Cordero and Cagan, 2010; Charlton-Perkins et al., 2011; Blackie et al., 2021). Although it is well established that Cut interacts with wingless and Notch signaling in the wing disc (Micchelli et al., 1997), evidence suggests that it doesn't interact with wingless in the eye disc (Cordero and Cagan, 2010). Cut's interactions with other genes in the retina therefore remain subject of further studies.

Importance of *cut* in SCs for accurate lens development

In *cut* knockdowns, we observed severe abnormalities in lens formation, with many parallel deformities in the two species that suggest a conserved overall function. Some differences, such as defects on the outer lens surfaces, are likely related to eye-type-specific differences in lens organization. Specifically, *D. melanogaster* eyes are characterized by biconvex lenses, whereas *T. marmoratus* eyes are characterized by plano convex lenses (Figure 1). These differences may have caused the fly eyes to show rough lens surfaces with prevalent holes (blueberry phenotype), whereas the beetle eyes maintained relatively smooth outer surfaces with only occasional dimples (Figure 3). However, knockdowns of *cut* in both species exhibited indentations on the inner lens surfaces as well as a generally disorganized lens arrays containing misshaped and fused lenses. As the inner surface is closer to the location of lens secretion (a process mediated by SCs and all pigment cells (Cagan and Ready, 1989; Wang et al., 2012; Chaturvedi et al., 2014; Stahl et al., 2017b), it isn't surprising that inner-surface deficits are more consistent between the two eye types. Similar accessory-cell based lens defects have already been observed in several *D. melanogaster* eye mutants (Higashijima et al., 1992; Charlton-Perkins et al., 2011; Wang et al., 2022). Of specific interest are the rough eye

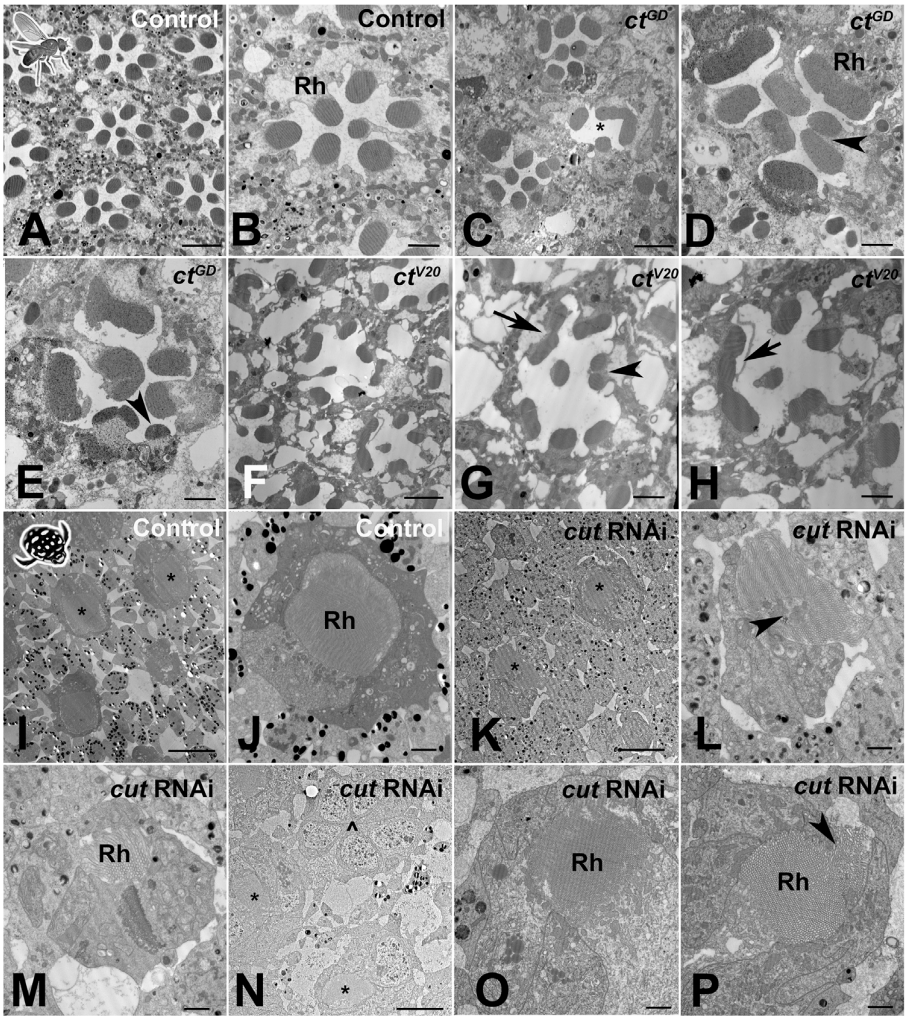

FIGURE 6
Cut knockdown leads to ultrastructural defects of rhabdoms in both eye types. **(A)**. As illustrated by a control individual, *D. melanogaster* has an open rhabdom that, at any cross-sectional plane, is formed by seven rhabdomeres. **(B)**. At higher magnification, it is apparent that the smaller central rhabdomere extends into the center of an extracellular lumen, which is bordered by larger and approximately evenly sized outer rhabdomeres. **(C)**. Overview of a ct^{GD} knockdown individual illustrates ommatidial displacements (with a compromised interommatidial space) and deformed or missing rhabdomeres (exemplified by the unit marked with *). **(D)**. Several units characterized by relatively extended or even split rhabdomeres (arrowhead). **(E)**. Other units showing unusually small rhabdomeres (arrowhead). **(F)**. Overview of a ct^{V20} knockdown individual illustrates ommatidia with relatively sparse rhabdomeres, large extracellular spaces between rhabdomeres, and sparse and degenerate interommatidial tissue. Non-etheless, ct^{V20} individuals also show laterally extended rhabdoms **(G)**, arrow, split rhabdomeres **(G)**, arrowhead, and possibly fused rhabdomeres **(H)**, arrow. **(I)**. As illustrated by a control individual, the superposition eyes of *T. marmoratus* are characterized by closed rhabdoms (two units with similar rhabdom diameters in close proximity are marked with *). **(J)** The rhabdom is positioned centrally within a healthy ommatidium. **(K)**. In *cut*RNAi individuals, neighboring units (marked with *) show relatively different rhabdom organization. **(L)** An unusually shaped rhabdom with central deficiencies. **(M)** A laterally displaced and strongly degenerate rhabdom. **(N)** Overview of several ommatidia in a different individual shows the complete absence of a rhabdom () next to two neighboring semi-intact rhabdoms (*). **(O)** A laterally degenerate rhabdom. **(P)** A rhabdom with a displaced portion (arrowhead). Scale bars = 5 μm **(A,C, F)**, 2 μm **(B, D, E, G, H, J, L, M, O, P)**, and 10 μm **(I, K, N)**; Rh = rhabdomere **(B, D)** or rhabdom **(J, M, O, P)**.

mutants of *prospero* and *pax2*, which specify SCs combinatorially (Charlton-Perkins et al., 2011), and *bar*, which is required for PPC function (Higashijima et al., 1992). Both these mutants and our knockdowns have irregularly shaped lens arrays, individual lenses with holes (including the blueberry phenotype), and flattened and fused lenses. These commonalities highlight the complexity of the process of proper lens formation, which involves many genes that act synergistically in multiple cell types.

Based on the severity of lens defects observed in both *cut* RNAi species, it is not surprising that we also noted major optical defects. In both species, lenses failed to form sharp images or to focus on the same plane, with associated variability in image magnification (Figure 4). Such optical assessments are a powerful but underutilized method for characterizing the functional deficits of lenses, although morphometric modeling (Wang et al., 2022) has been implemented as an alternative assessment method. The

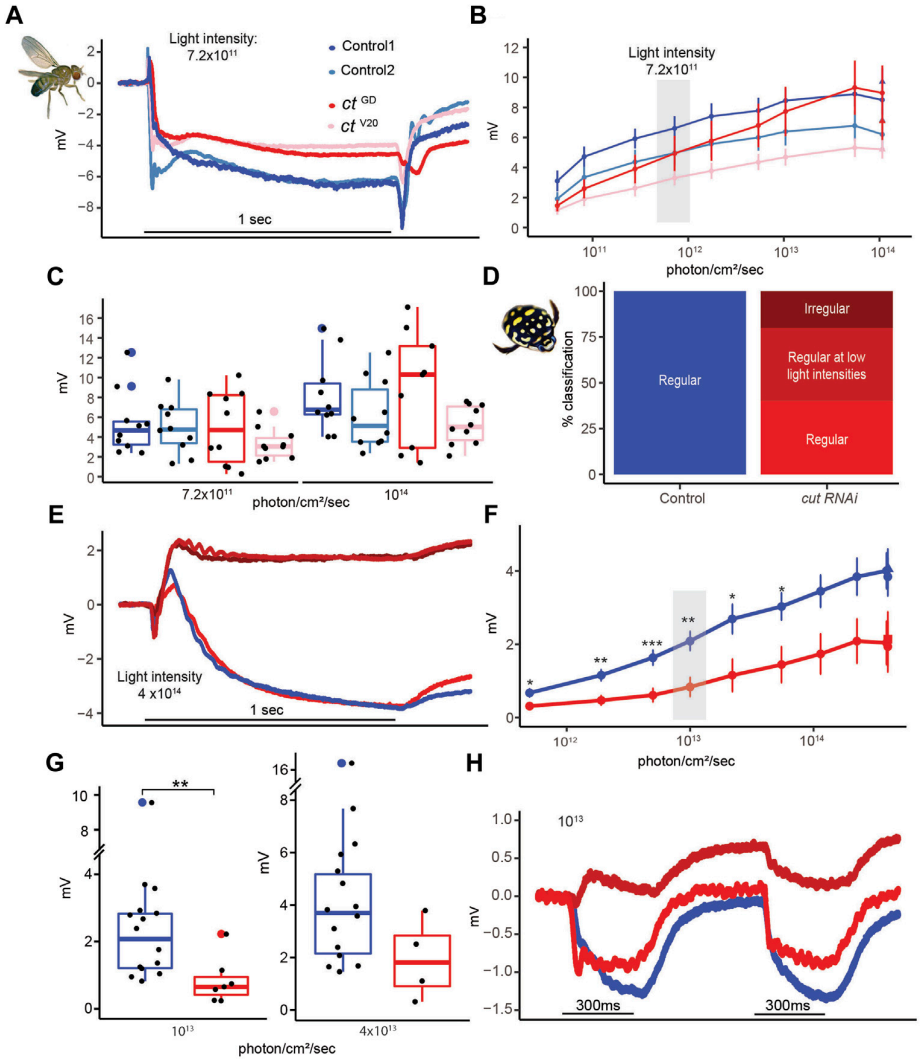

FIGURE 7
Despite major structural deficits, electroretinograms of *cut* knockdown individuals show relatively intact physiological responses in *D. melanogaster* and relatively minor deficiencies in *T. marmoratus*. **(A)**. Example recordings from two control and two test flies illustrate comparable responses. **(B)**. Average responses (with standard error) to increasing light intensities suggest a comparable dynamic range across the four tested fly lines (n = 10 each). **(C)**. Example responses at two different light intensities. **(D)**. Quantification of *cut*RNAi injected beetles shows inverted responses at all (dark red) or higher (medium red) light intensities. **(E)**. Example recordings of a control individual and one of each of the three phenotypes in **(D)**. **(F)**. Average responses (with standard error) to increasing light intensities suggest a comparable dynamic range between control and *cut*RNAi individuals, albeit with generally lower responses in the knockdowns (*p < 0.05, **p < 0.005; based on Wilcoxon's rank sum test). **(G)**. Example responses at two different light intensities. **(H)**. Example of *cut*RNAi individuals showing different response dynamics when multiple pulses are presented.

observed optical deficits likely have dramatic implications on the spatial resolution of both compound eye types. It remains an open question whether *cut* knockdowns also affect the optics of the crystalline cone (CC), another important extracellular optical component of superposition eyes (Warrant and McIntyre, 1993; Meece et al., 2021). The CC, which re-inverts the image to allow for an upright image at the level of PRs, is likely also formed (or at least contributed to) by SCs (Nilsson, 1989). Unfortunately, unlike in other beetles, such as fireflies, in *T. marmoratus*, the CCs aren't retained when isolating lenses and hence cannot be optically assessed.

Importance of *cut* in SCs for PR placement and rhabdomere morphology, with minimal effects on PR function

Although Cut affects SCs, *cut*RNAi individuals of both species also exhibit severe morphological defects in adjacent PR cells. On a gross morphological level, this includes laterally displaced rhabdoms that are already apparent in early development (Figure 2) as well as longitudinally displaced PR nuclei, shortened rhabdoms, and rhabdoms that extend through the basement membrane (Figure 5). In *D. melanogaster*, the latter two phenotypes are particularly severe.

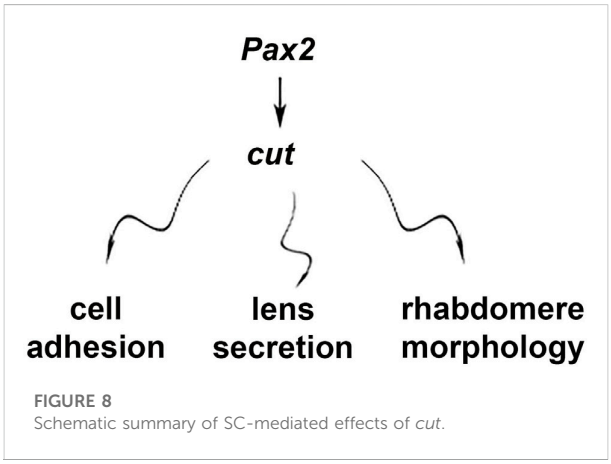

FIGURE 8
Schematic summary of SC-mediated effects of *cut*.

Notably in that species the orientation of rhabdomeres turns during development (Ready, 2002). It is possible that observed phenotypes relate to perturbations of that process, a possibility that warrants further investigation. These observed differences could be related to variations in the knockdown severity but could also be related to organizational differences between the two eye types, with rhabdoms in beetles originating much deeper in the eye but terminating more distal to the basement membrane than those in flies. Parallel defects were also observed in cross-sections at the ultrastructural level, with rhabdoms of both species showing a variety of morphological defects including splitting, variable sizing, and lateral displacements (Figure 6). In *D. melanogaster,* where the open rhabdom facilitates checking for the presence of all rhabdomeres, a few ommatidia appear to be missing some rhabdomeres. However, they could also have been displaced to a different plane; evaluation of this possibility requires future 3D TEM analysis. Our data is consistent with a growing body of evidence that raises the possibility that an intact SC–PR interface is necessary for proper PR placement (during early pupation) and rhabdom elongation (during mid to late pupation (Longley and Ready, 1995). It is noteworthy that SC-specific *pax2* RNAi flies have very similar patterning defects (Fu and Noll, 1997; Charlton-Perkins et al., 2017), as might be expected if these two genes act through a common pathway. In contrast, Blimp-1 knockdown in SCs also leads to eyes with shortened rhabdoms (Wang et al., 2022), although they do not cross the basement membrane. Interestingly, even defects in surrounding support cells, such as PPCs, have been reported to result in similar rhabdom deficiencies in flies, seen in Bar mutants (Higashijima et al., 1992). Overall, these findings indicate that the accurate patterning of SCs is necessary to allow PRs to be properly shaped and positioned. It has already been demonstrated that ineffective cell adhesion in PRs is a major contributor (Longley and Ready, 1995; Izaddoost et al., 2002), a topic that warrants further exploration.

In line with our interpretation that structural PR deficits in *cut* knockdown flies and beetles are secondary to disturbances of the entire ommatidial unit, we found that the physiological response of PRs was relatively intact, although there were notable phenotype differences between the two species. In *D. melanogaster*, the *cut*RNAi flies had normal responses despite abnormal morphology, similar to SC-specific *pax2* knockdown flies (Charlton-Perkins et al., 2017). The possible physiological phenotypes in flies are worth further investigation, as our study was hampered by a relatively large variation in responses, likely due to minor differences in eye color, and more subtle physiological deficits may only become apparent when PRs are substantially challenged (Riazuddin et al., 2012; Charlton-Perkins et al., 2017).

In contrast to flies, the PR responses in *cut*RNAi beetles were significantly lower than those in the controls for some light intensities and were even inverted in many cases (Figure 7). This seemingly reversed phenotype is reminiscent of that of *repo* (a general glial marker) mutant flies (Xiong et al., 1994). Since in contrast to *D. melanogaster*, the effect of RNAi in *T. marmoratus* wasn't cell type specific, it is conceivable that the observed species-specific differences are related to *cut*-dependent roles in other cell types such as the subretinal glia (Bauke et al., 2015). Interestingly, the reversed response was sometimes transient, being present only in the first pulse (Figure 7). As the ERG is a field potential measured from the surface of the eye (Belusic, 2011), this waveform could be related to defects in the resistance barrier and the complex flow of currents in the relatively tight spaces of the eye rather than an altered PR response.

A glimpse into the complex genetic basis of eye diversification

The data presented here identify *cut* as part of a support-cell-specific conserved gene network that is essential for proper eye development in different compound eye types, with largely parallel phenotypes in *cut* knockdowns in flies and beetles. Interestingly, several defects observed here parallel those in SC-*pax2* mutants, thus providing supportive functional evidence for a *pax2-cut* model in SCs that is essential for proper cell adhesion, lens secretion, and PR morphology (Figure 8). Here, we studied these knockdown phenotypes for the first time within the framework of a direct comparison between eye types, laying the groundwork for further investigations into this model and how it might regulate the development of different compound eyes. Since diverse compound eyes, including those with different optics, are composed of ommatidia with highly conserved cellular compositions (Paulus, 1979; Nilsson, 1989), it is not surprising that the disruption of a central cell type, such as SCs, has dramatic effects on the entire complex ommatidial unit.

However, the manner in which related deficits manifest could be, at least to some degree, eye type specific. For example, we expect deficits to be particularly detrimental for the superposition optics of beetles, as a high level of precision in organization is required for proper function. Our data suggest that *cut*RNAi in beetles destabilizes this precision in multiple ways, including affecting ommatidial array regularity, lens integrity and optics, clear zone integrity, and PR placement. As each of these factors could itself be detrimental to proper function, we expect that even a relatively mild *cut* knockdown phenotype would lead to relatively dramatic visual deficits, with the potential of completely losing the ability to resolve images. For *D. melanogaster* eyes, the loss of spatial resolution is also expected, but this effect may be more subtle, as in parts of the eye, individual lenses would continue to project images (albeit possibly blurry images) on the corresponding PRs. Additionally, both eye types are typical for flying insects that capitalize on precise sampling

from neighboring units for proper motion computation, which generally relies on elementary motion detectors (for a review, see (Egelhaaf et al., 1988). Hence, even subtle phenotypes are expected to lead to specific deficits, which is an interesting area for further investigation.

Although this study compared two optically relatively different compound eye types, we have only scratched the surface of how Cut may be involved in the incredible diversity of eyes that have evolved in the lineage of compound eyes (Buschbeck, 2014; Morehouse et al., 2017; Lavin et al., 2022) and are composed of a set of highly conserved cell types (Paulus, 1979). One particularly intriguing observation in our study is the occurrence of fused lenses, which are particularly significant from an optical perspective, as such fusion events may give rise to eye formations in which one lens serves multiple PRs, the hallmark of a single-chamber, image-forming eye. Transitions from compound eyes to image-forming eyes have been observed in nature (for example, in mysid shrimp (Nilsson and Modlin, 1994) but have thus far remained unexplored from a genetic perspective. We anticipate that our study is part of the groundwork for further explorations on support-cell-mediated eye diversification and how deeply conserved eye development genes beyond the RDGN contribute to the manifestation of optically highly diverse eye types.

Data availability statement

The original contributions presented in the study are included in the article/Supplementary Material, further inquiries can be directed to the corresponding authors.

Author contributions

Conceptualization: SR, EB, and TC; investigation: SR, MC-P, and MM; methodology: SR, EB, and TC; formal analysis: SR data curation: SR, EB, and TC; writing—original draft: SR and EB; writing—review and editing: SR, EB, TC, and MC-P; supervision: EB and TC; funding acquisition: EB and TC.

Funding

This research was funded by the National Science Foundation under IOS-1856241 (EB), the National Institutes of Health grants R21-EY031526, EY024404, and unrestricted funds from Research to Prevent Blindness (TC), and Cincinnati Children's Hospital Medical Center (MC-P).

Acknowledgments

We thank Dr. John Mast for initial characterization of the *D. melanogaster* ct^{GD} phenotype and Dr. Aaron Stahl for the initial efforts in identifying and cloning *cut* in *T. marmoratus*; the beetle care team of the EB laboratory for helping with insect rearing; the Bloomington *Drosophila* Stock Center and Vienna *Drosophila* Resource Center for providing flies; Chet Closson and the Live Microscopy Core, College of Medicine (University of Cincinnati) for help with confocal imaging; the CCHMC Pathology Core for TEM imaging, with special thanks to Birgit Ehmer and Jessica Webster; Melodie Fickenscher and CEAC (University of Cincinnati) for SEM imaging; and Tamara Pace for editorial help.

Conflict of interest

The authors declare that the research was conducted in the absence of any commercial or financial relationships that could be construed as a potential conflict of interest.

Publisher's note

All claims expressed in this article are solely those of the authors and do not necessarily represent those of their affiliated organizations, or those of the publisher, the editors and the reviewers. Any product that may be evaluated in this article, or claim that may be made by its manufacturer, is not guaranteed or endorsed by the publisher.

Supplementary material

The Supplementary Material for this article can be found online at: https://www.frontiersin.org/articles/10.3389/fcell.2023.1104620/full#supplementary-material

References

Agi, E., Langen, M., Altschuler, S. J., Wu, L. F., Zimmermann, T., and Hiesinger, P. R. (2014). The evolution and development of neural superposition. *J. Neurogenetics* 28, 216–232. doi:10.3109/01677063.2014.922557

Bauke, A-C., Sasse, S., Matzat, T., and Klämbt, C. (2015). A transcriptional network controlling glial development in the *Drosophila* visual system. *Development* 142, 2184–2193. doi:10.1242/dev.119750

Belušič, G. (2011). "ERG in Drosophila," in *Electroretinograms*. Editor G. Belušič (London: IntecOpen). doi:10.5772/21747

Blackie, L., Walther, R. F., Staddon, M. F., Banerjee, S., and Pichaud, F. (2020). Cell-type-specific mechanical response and myosin dynamics during retinal lens development in *Drosophila*. *Mol. Biol. Cell.* 31, 1355–1369. doi:10.1091/mbc.E19-09-0523

Blackie, L., Tozluoglu, M., Trylinski, M., Walther, R. F., Schweisguth, F., Mao, Y., et al. (2021). A combination of Notch signaling, preferential adhesion and endocytosis induces a slow mode of cell intercalation in the *Drosophila* retina. *Development* 148, 197301. doi:10.1242/dev.197301

Blochlinger, K., Bodmer, R., Jan, L. Y., and Jan, Y. N. (1990). Patterns of expression of cut, a protein required for external sensory organ development in wild-type and cut mutant *Drosophila* embryos. *Genes. and Dev.* 4, 1322–1331. doi:10.1101/gad.4.8.1322

Blochlinger, K., Jan, L. Y., and Jan, Y. N. (1991). Transformation of sensory organ identity by ectopic expression of Cut in Drosophila. *Genes. and Dev.* 5, 1124–1135. doi:10.1101/gad.5.7.1124

Blochlinger, K., Jan, L. Y., and Jan, Y. N. (1993). Postembryonic patterns of expression of cut, a locus regulating sensory organ identity in *Drosophila*. *Development* 117, 441–450. doi:10.1242/dev.117.2.441

Burns, K. A., Gutzwiller, L. M., Tomoyasu, Y., and Gebelein, B. (2012). Oenocyte development in the red flour beetle *Tribolium castaneum*. *Dev. Genes. Evol.* 222, 77–88. doi:10.1007/s00427-012-0390-z

Buschbeck, E. K., and Friedrich, M. (2008). Evolution of insect eyes: Tales of ancient heritage, deconstruction, reconstruction, remodeling, and recycling. *Evol. Educ. Outreach* 1, 448–462. doi:10.1007/s12052-008-0086-z

Buschbeck, E., Ehmer, B., and Hoy, R. (1999). Chunk versus point sampling: Visual imaging in a small insect. *Science* 286, 1178–1180. doi:10.1126/science.286.5442.1178

Buschbeck, E. K. (2014). Escaping compound eye ancestry: The evolution of single-chamber eyes in holometabolous larvae. *J. Exp. Biol.* 217, 2818–2824. doi:10.1242/jeb.085365

Cagan, R. L., and Ready, D. F. (1989). The emergence of order in the *Drosophila* pupal retina. *Dev. Biol.* 136, 346–362. doi:10.1016/0012-1606(89)90261-3

Canon, J., and Banerjee, U. (2003). *In vivo* analysis of a developmental circuit for direct transcriptional activation and repression in the same cell by a Runx protein. *Genes. and Dev.* 17, 838–843. doi:10.1101/gad.1064803

Chan, E. H., Chavadimane Shivakumar, P., Clément, R., Laugier, E., and Lenne, P-F. (2017). Patterned cortical tension mediated by N-cadherin controls cell geometric order in the *Drosophila* eye. *eLife* 6, e22796. doi:10.7554/eLife.22796

Charlton-Perkins, M., and Cook, T. A. (2010). Building a fly eye: Terminal differentiation events of the retina, corneal lens, and pigmented epithelia. *Curr. Top. Dev. Biol.* 93, 129–173. doi:10.1016/B978-0-12-385044-7.00005-9

Charlton-Perkins, M., Leigh Whitaker, S., Fei, Y., Xie, B., Li-Kroeger, D., Gebelein, B., et al. (2011). Prospero and Pax2 combinatorially control neural cell fate decisions by modulating Ras- and Notch-dependent signaling. *Neural Dev.* 6, 20. doi:10.1186/1749-8104-6-20

Charlton-Perkins, M. A., Sendler, E. D., Buschbeck, E. K., and Cook, T. A. (2017). Multifunctional glial support by Semper cells in the *Drosophila* retina. *PLoS Genet.* 13, e1006782. doi:10.1371/journal.pgen.1006782

Charlton-Perkins, M. A., Friedrich, M., and Cook, T. A. (2021). Semper's cells in the insect compound eye: Insights into ocular form and function. *Dev. Biol.* 479, 126–138. doi:10.1016/j.ydbio.2021.07.015

Chaturvedi, R., Reddig, K., and Li, H-S. (2014). Long-distance mechanism of neurotransmitter recycling mediated by glial network facilitates visual function in *Drosophila*. *Proc. Natl. Acad. Sci. U. S. A.* 111, 2812–2817. doi:10.1073/pnas.1323714111

Cordero, J. B., and Cagan, R. L. (2010). Canonical wingless signaling regulates cone cell specification in the *Drosophila* retina. *Dev. Dyn.* 239, 875–884. doi:10.1002/dvdy.22235

Corty, M. M., Tam, J., and Grueber, W. B. (2016). Dendritic diversification through transcription factor-mediated suppression of alternative morphologies. *Development* 143, 1351–1362. doi:10.1242/dev.130906

Cronin, T. W., Johnsen, S., Justin Marshall, N., and Warrant, E. J. (2014). *Visual ecology*.

Ebacher, D. J. S., Todi, S. V., Eberl, D. F., and Boekhoff-Falk, G. E. (2007). Cut mutant *Drosophila* auditory organs differentiate abnormally and degenerate. *Fly* 1, 86–94. doi:10.4161/fly.4242

Egelhaaf, M., Hausen, K., Reichardt, W., and Wehrhahn, C. (1988). Visual course control in flies relies on neuronal computation of object and background motion. *Trends Neurosci.* 11, 351–358. doi:10.1016/0166-2236(88)90057-4

Friedrich, M. (2003). Evolution of insect eye development: First insights from fruit fly, grasshopper and flour beetle. *Integr. Comp. Biol.* 43, 508–521. doi:10.1093/icb/43.4.508

Fu, W., and Noll, M. (1997). The Pax2 homolog sparkling is required for development of cone and pigment cells in the *Drosophila* eye. *Genes. and Dev.* 11, 2066–2078. doi:10.1101/gad.11.16.2066

Gainett, G., Ballesteros, J. A., Kanzler, C. R., Zehms, J. T., Zern, J. M., Aharon, S., et al. (2020). Systemic paralogy and function of retinal determination network homologs in arachnids. *BMC Genomics* 21, 811. doi:10.1186/s12864-020-07149-x

Gehring, W. J. (2001). The genetic control of eye development and its implications for the evolution of the various eye-types. *Zoology* 104, 171–183. doi:10.1078/0944-2006-00022

Grillo-Hill, B. K., and Wolff, T. (2009). Dynamic cell shapes and contacts in the developing Drosophila retina are regulated by the Ig cell adhesion protein hibris. *Dev. Dyn.* 238, 2223–2234. doi:10.1002/dvdy.21981

Hardiman, K. E., Brewster, R., Khan, S. M., Deo, M., and Bodmer, R. (2002). The bereft gene, a potential target of the neural selector gene cut, contributes to bristle morphogenesis. *Genetics* 161, 231–247. doi:10.1093/genetics/161.1.231

Hayashi, T., and Carthew, R. W. (2004). Surface mechanics mediate pattern formation in the developing retina. *Nature* 431, 647–652. doi:10.1038/nature02952

Higashijima, S., Kojima, T., Michiue, T., Ishimaru, S., Emori, Y., and Saigo, K. (1992). Dual Bar homeo box genes of *Drosophila* required in two photoreceptor cells, R1 and R6, and primary pigment cells for normal eye development. *Genes. and Dev.* 6, 50–60. doi:10.1101/gad.6.1.50

Homann, H. (1924). Zum Problem der Ocellenfunktion bei den Insekten. *Z. für Vgl. Physiol.* 1, 541–578. doi:10.1007/bf00337911

Hsiung, F., and Moses, K. (2002). Retinal development in *Drosophila*: Specifying the first neuron. *Hum. Mol. Genet.* 11, 1207–1214. doi:10.1093/hmg/11.10.1207

Iyer, J., Wang, Q., Le, T., Pizzo, L., Gronke, S., Ambegaokar, S. S., et al. (2016). Quantitative assessment of eye phenotypes for functional genetic studies using *Drosophila melanogaster*. *G3* 6, 1427–1437. doi:10.1534/g3.116.027060

Izaddoost, S., Nam, S-C., Bhat, M. A., Bellen, H. J., and Choi, K-W. (2002). *Drosophila* Crumbs is a positional cue in photoreceptor adherens junctions and rhabdomeres. *Nature* 416, 178–183. doi:10.1038/nature720

Klann, M., and Seaver, E. C. (2019). Functional role of pax6 during eye and nervous system development in the annelid *Capitella teleta*. *Dev. Biol.* 456, 86–103. doi:10.1016/j.ydbio.2019.08.011

Klann, M., Schacht, M. I., Benton, M. A., and Stollewerk, A. (2021). Functional analysis of sense organ specification in the *Tribolium castaneum* larva reveals divergent mechanisms in insects. *BMC Biol.* 19, 22. doi:10.1186/s12915-021-00948-y

Kumar, J. P., and Moses, K. (2001). Expression of evolutionarily conserved eye specification genes during *Drosophila* embryogenesis. *Dev. Genes. Evol.* 211, 406–414. doi:10.1007/s004270100177

Kumar, J. P. (2001). Signalling pathways in *Drosophila* and vertebrate retinal development. *Nat. Rev. Genet.* 2, 846–857. doi:10.1038/35098564

Kumar, J. P. (2012). Building an ommatidium one cell at a time. *Dev. Dyn.* 241, 136–149. doi:10.1002/dvdy.23707

Land, M. F., and Nilsson, D-E. (2012). *Animal eyes*.

Lavin, R., Rathore, S., Bauer, B., Disalvo, J., Mosley, N., Shearer, E., et al. (2022). EyeVolve, a modular PYTHON based model for simulating developmental eye type diversification. *Front. Cell. Dev. Biol.* 10, 964746. doi:10.3389/fcell.2022.964746

Longley, R. L., Jr, and Ready, D. F. (1995). Integrins and the development of three-dimensional structure in the *Drosophila* compound eye. *Dev. Biol.* 171, 415–433. doi:10.1006/dbio.1995.1292

Maksimovic, S., Layne, J. E., and Buschbeck, E. K. (2011). Spectral sensitivity of the principal eyes of sunburst diving beetle, *Thermonectus marmoratus* (Coleoptera: Dytiscidae), larvae. *J. Exp. Biol.* 214, 3524–3531. doi:10.1242/jeb.058990

Meece, M., Rathore, S., and Buschbeck, E. K. (2021). Stark trade-offs and elegant solutions in arthropod visual systems. *J. Exp. Biol.* 224, jeb215541. doi:10.1242/jeb.215541

Meyer-Rochow, V. B. (2015). Compound eyes of insects and crustaceans: Some examples that show there is still a lot of work left to be done. *Insect Sci.* 22, 461–481. doi:10.1111/1744-7917.12117

Micchelli, C. A., Rulifson, E. J., and Blair, S. S. (1997). The function and regulation of cut expression on the wing margin of *Drosophila*: Notch, Wingless and a dominant negative role for Delta and Serrate. *Development* 124, 1485–1495. doi:10.1242/dev.124.8.1485

Miguel, C., de Miguel, C., Linsler, F., Casanova, J., and Franch-Marro, X. (2016). Genetic basis for the evolution of organ morphogenesis: The case of spalt and cut in the development of insect trachea. *Development* 143, 3615–3622. doi:10.1242/dev.134924

Mishra, A. K., and Sprecher, S. G. (2020). "Early eye development: Specification and determination," in *Molecular genetics of axial patterning, growth and disease in Drosophila eye*, 1–52.

Morehouse, N. I., Buschbeck, E. K., Zurek, D. B., Steck, M., and Porter, M. L. (2017). Molecular evolution of spider vision: New opportunities, familiar players. *Biol. Bull.* 233, 21–38. doi:10.1086/693977

Morrison, C. A., Chen, H., Cook, T., Brown, S., and Treisman, J. E. (2018). Glass promotes the differentiation of neuronal and non-neuronal cell types in the *Drosophila* eye. *PLoS Genet.* 14, e1007173. doi:10.1371/journal.pgen.1007173

Nagaraj, R., and Banerjee, U. (2007). Combinatorial signaling in the specification of primary pigment cells in the *Drosophila* eye. *Development* 134, 825–831. doi:10.1242/dev.02788

Nepveu, A. (2001). Role of the multifunctional CDP/Cut/Cux homeodomain transcription factor in regulating differentiation, cell growth and development. *Gene* 270, 1–15. doi:10.1016/s0378-1119(01)00485-1

Nilsson, D. E., and Modlin, R. (1994). A mysid shrimp carrying a pair of binoculars. *J. Exp. Biol.* 189, 213–236. doi:10.1242/jeb.189.1.213

Nilsson, D-E. (1983). Evolutionary links between apposition and superposition optics in crustacean eyes. *Nature* 302, 818–821. doi:10.1038/302818a0

Nilsson, D-E. (1989). "Optics and evolution of the compound eye," in *Facets of vision* (Springer Berlin Heidelberg), 30–73.

Nilsson, D-E. (2021). The diversity of eyes and vision. *Annu. Rev. Vis. Sci.* 7, 19–41. doi:10.1146/annurev-vision-121820-074736

O'Shea, M., and Adams, M. E. (1981). Pentapeptide (proctolin) associated with an identified neuron. *Science* 213, 567–569. doi:10.1126/science.6113690

Paulus, H. F. (1979). "Eye structure and the monophyly of the Arthropoda," in *Arthropod phylogeny*. Editor A. P. Gupta (New York: Van Nostrad Reinhold), 299–384.

Perry, M., Kinoshita, M., Saldi, G., Huo, L., Arikawa, K., and Desplan, C. (2016). Molecular logic behind the three-way stochastic choices that expand butterfly colour vision. *Nature* 535, 280–284. doi:10.1038/nature18616

Querenet, M., Goubard, V., Chatelain, G., Davoust, N., and Mollereau, B. (2015). Spen is required for pigment cell survival during pupal development in *Drosophila*. *Dev. Biol.* 402, 208–215. doi:10.1016/j.ydbio.2015.03.021

Rathore, S., Hassert, J., Clark-Hachtel, C. M., Stahl, A., Tomoyasu, Y., and Bushbeck, E. K. (2020). RNA interference in aquatic beetles as a powerful tool for manipulating gene expression at specific developmental time points. *J. Vis. Exp.* 159, e61477. doi:10.3791/61477

Ready, D. F. (2002). *Drosophila* compound eye morphogenesis: Blind mechanical engineers? *Results Problems Cell. Differ.* 37, 191–204. doi:10.1007/978-3-540-45398-7_12

Riazuddin, S., Belyantseva, I. A., Giese, A. P. J., Lee, K., Indzhykulian, A. A., Nandamuri, S. P., et al. (2012). Alterations of the CIB2 calcium- and integrin-binding protein cause Usher syndrome type 1J and nonsyndromic deafness DFNB48. *Nat. Genet.* 44, 1265–1271. doi:10.1038/ng.2426

Richter, S. (2002). The tetraconata concept: Hexapod-crustacean relationships and the phylogeny of Crustacea. *Org. Divers. Evol.* 2, 217–237. doi:10.1078/1439-6092-00048

Samadi, L., Schmid, A., and Eriksson, B. J. (2015). Differential expression of retinal determination genes in the principal and secondary eyes of Cupiennius salei Keyserling (1877). *Evodevo* 6, 16. doi:10.1186/s13227-015-0010-x

Scholtz, G., Staude, A., and Dunlop, J. A. (2019). Trilobite compound eyes with crystalline cones and rhabdoms show mandibulate affinities. *Nat. Commun.* 10, 2503. doi:10.1038/s41467-019-10459-8

Schomburg, C., Turetzek, N., Schacht, M. I., Schneider, J., Kirfel, P., Prpic, N.-M., et al. (2015). Molecular characterization and embryonic origin of the eyes in the common house spider Parasteatoda tepidariorum. *Evodevo* 6, 15. doi:10.1186/s13227-015-0011-9

Schwentner, M., Richter, S., Rogers, D. C., and Giribet, G. (2018). Tetraconatan phylogeny with special focus on malacostraca and branchiopoda: Highlighting the strength of taxon-specific matrices in phylogenomics. *Proc. R. Soc. B* 285, 20181524. doi:10.1098/rspb.2018.1524

Sharkey, C. R., Blanco, J., Leibowitz, M. M., Pinto-Benito, D., and Wardill, T. J. (2020). The spectral sensitivity of *Drosophila* photoreceptors. *Sci. Rep.* 10, 18242. doi:10.1038/s41598-020-74742-1

Stahl, A. L., Baucom, R. S., Cook, T. A., and Buschbeck, E. K. (2017a). A complex lens for a complex eye. *Integr. Comp. Biol.* 57, 1071–1081. doi:10.1093/icb/icx116

Stahl, A. L., Charlton-Perkins, M., Buschbeck, E. K., and Cook, T. A. (2017b). The cuticular nature of corneal lenses in *Drosophila melanogaster*. *Dev. Genes. Evol.* 227, 271–278. doi:10.1007/s00427-017-0582-7

Stegeman, R., Hall, H., Escobedo, S. E., Chang, H. C., and Weake, V. M. (2018). Proper splicing contributes to visual function in the aging *Drosophila* eye. *Aging Cell.* 17, e12817. doi:10.1111/acel.12817

Stowasser, A., and Buschbeck, E. K. (2012). Electrophysiological evidence for polarization sensitivity in the camera-type eyes of the aquatic predacious insect larva *Thermonectus marmoratus*. *J. Exp. Biol.* 215, 3577–3586. doi:10.1242/jeb.075028

Stowasser, A., Rapaport, A., Layne, J. E., Morgan, R. C., and Buschbeck, E. K. (2010). Biological bifocal lenses with image separation. *Curr. Biol. CB* 20, 1482–1486. doi:10.1016/j.cub.2010.07.012

Tea, J. S., Cespedes, A., Dawson, D., Banerjee, U., and Call, G. B. (2014). Dissection and mounting of *Drosophila* pupal eye discs. *J. Vis. Exp.* 93, e52315. doi:10.3791/52315

Waddington, C. H., and Perry, M. (1960). The ultra-structure of the developing eye of *Drosophila*. *Proc. R. Soc. Lond. B* 153, 155–178. doi:10.1098/rspb.1960.0094

Wang, X., Wang, T., Ni, J. D., von Lintig, J., and Montell, C. (2012). The *Drosophila* visual cycle and de novo chromophore synthesis depends on rdhB. *J. Neurosci.* 32, 3485–3491. doi:10.1523/JNEUROSCI.5350-11.2012

Wang, H., Morrison, C. A., Ghosh, N., Tea, J. S., Call, G. B., and Treisman, J. E. (2022). The Blimp-1 transcription factor acts in non-neuronal cells to regulate terminal differentiation of the *Drosophila* eye. *Development* 149, dev.200217. doi:10.1242/dev.200217

Warrant, E. J., and McIntyre, P. D. (1993). Arthropod eye design and the physical limits to spatial resolving power. *Prog. Neurobiol.* 40, 413–461. doi:10.1016/0301-0082(93)90017-m

Warrant, E. J., Kelber, A., Wallén, R., and Wcislo, W. T. (2006). Ocellar optics in nocturnal and diurnal bees and wasps. *Arthropod Struct. Dev.* 35, 293–305. doi:10.1016/j.asd.2006.08.012

Warrant, E. J. (1999). Seeing better at night: Life style, eye design and the optimum strategy of spatial and temporal summation. *Vis. Res.* 39, 1611–1630. doi:10.1016/s0042-6989(98)00262-4

Wilson, M. (1978). The functional organisation of locust ocelli. *J. Comp. Physiology A* 124, 297–316. doi:10.1007/bf00661380

Wolff, T. (2011). Preparation of *Drosophila* eye specimens for transmission electron microscopy. *Cold Spring Harb. Protoc.* 2011, 1386–1388. doi:10.1101/pdb.prot066514

Xiong, W. C., Okano, H., Patel, N. H., Blendy, J. A., and Montell, C. (1994). Repo encodes a glial-specific homeo domain protein required in the *Drosophila* nervous system. *Genes. and Dev.* 8, 981–994. doi:10.1101/gad.8.8.981

Yang, X., Weber, M., Zarinkamar, N., Posnien, N., Friedrich, F., Wigand, B., et al. (2009a). Probing the *Drosophila* retinal determination gene network in *Tribolium* (II): The Pax6 genes eyeless and twin of eyeless. *Dev. Biol.* 333, 215–227. doi:10.1016/j.ydbio.2009.06.013

Yang, X., Zarinkamar, N., Bao, R., and Friedrich, M. (2009b). Probing the *Drosophila* retinal determination gene network in *Tribolium* (I): The early retinal genes dachshund, eyes absent and sine oculis. *Dev. Biol.* 333, 202–214. doi:10.1016/j.ydbio.2009.02.040